Implementation of temperature dependant thermo-optical properties and complex 3D geometries in ESATAN-TMS

Simone Del Togno[1]
German Aerospace Center, Berlin, 12489, Germany

Henri Brouquet[2]
ITP Engines UK, Whetstone, Leicester, LE86LH, United Kingdom

and

Gabriele Messina[3]
German Aerospace Center, Berlin, 12489, Germany

Radiative heat transfer plays a major role in the thermal behavior of any space application compared to a typical Earth-based system. Space systems are known to operate in an environment characterized by a wide range of temperatures and heat loads, such as planetary and solar fluxes or deep space, planet and sun temperature. All these factors will critically impact upon the thermal design of spacecraft and special thermal coatings are generally used in thermal control. Many of these coatings present temperature dependent thermo-optical properties, which cannot be neglected in the design of space systems. However, in most thermal models, the temperature dependence is often reduced to the definition of two sets of properties, namely the IR and UV ranges.

In addition, space systems usually present complex 3D geometries like antennas, optical devices or reflective baffles. For such components, the thermal behaviour is generally strongly coupled to their geometry, for instance the amount of rejected environmental radiation of a reflective baffle depends upon the shape of its reflective surfaces. It is therefore essential to model their surfaces with high accuracy. Unfortunately, complex shapes are often not fully implemented in thermal software.

The objective of this paper is to present a general method to implement temperature dependant thermo-optical properties and to approximate complex 3D geometry using ESATAN-TMS, the European standard thermal analysis package.

Practical applications for current space missions will be used to illustrate both methods and a comparison between different models will be presented to show the high inaccuracy that occurs when temperature dependencies are neglected.

---

[1] Thermal engineer, Institute for Planetary Research, German Aerospace Center, Berlin, 12489, Germany, AIAA Member (MB)

[2] Group Head Thermal Engineering and Software Product, ITP Engines UK, Whetstone, Leicester, LE86LH, United Kingdom, AIAA Member (MB)

[3] Thermal architect, Institute for Planetary Research, German Aerospace Center, Berlin, 12489, Germany, AIAA Member (MB)

American Institute of Aeronautics and Astronautics

Nomenclature

A	=	area
a, b, c	=	geometrical parameters
α, β, γ	=	geometrical parameters
α	=	absorptivity
c	=	speed of light
Δt	=	time interval
e	=	Euler's number
ε	=	emissivity
f, F, Φ	=	generic functions
η	=	generic thermo-optical property
GMM	=	geometrical mathematical model
GR	=	radiative exchange factor
GUI	=	graphical user interface
GV	=	view factor
h	=	Planck constant
I	=	intensity of radiation
IR	=	infra red
φ, q	=	heat flux
k	=	Boltzmann constant
l	=	length
λ	=	wavelength
P	=	point
QE	=	planetary IR flux
r	=	radius
REF	=	radiative exchange factor
σ	=	Stefan-Boltzmann constant
ξ	=	error
ξ_{MAX}	=	max allowable error
t	=	time
T	=	temperature
T_{BODY}	=	temperature of the body
T_{EQ}	=	equivalent temperature
TMM	=	thermal mathematical model
τ	=	time period
UV	=	solar waveband (ultraviolet and visible)
y	=	generic function
ψ_i, Ψ	=	approximating functions
x_i	=	position of the node i in x direction
x_i'	=	iterated position of the node i in x direction

I. Temperature dependant thermo-optical properties

THE thermo-optical properties of the surfaces of one thermal system influence two different aspects of the related mathematical problem: the radiative heat exchange between elements of the system and the environmental fluxes striking the components of system. The optical properties of any material, coating or surface are expressed in terms of spectrum (Figure 1).
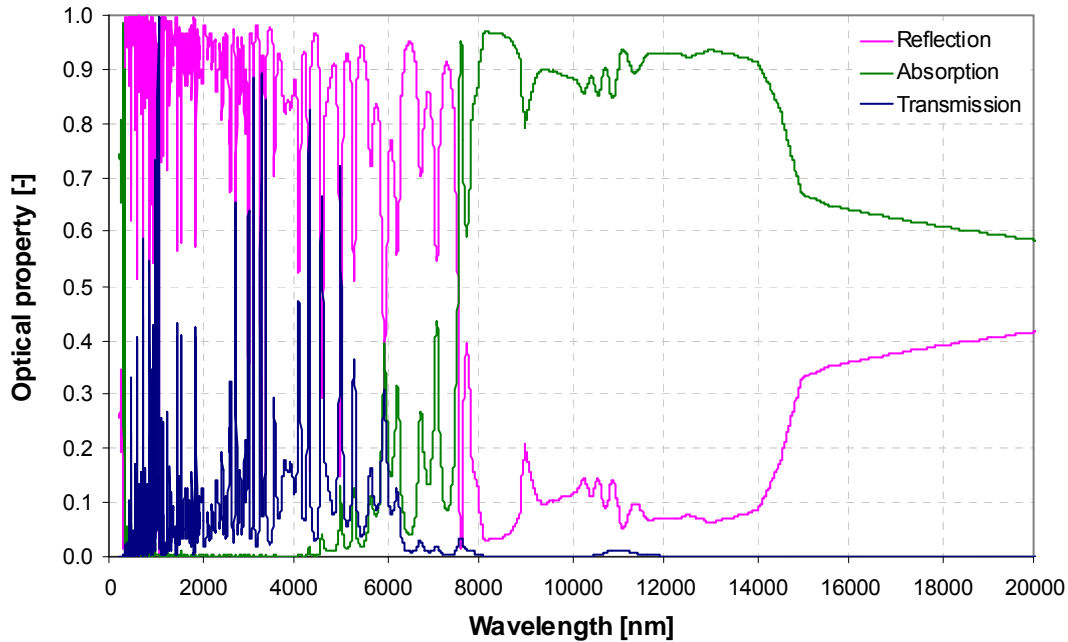
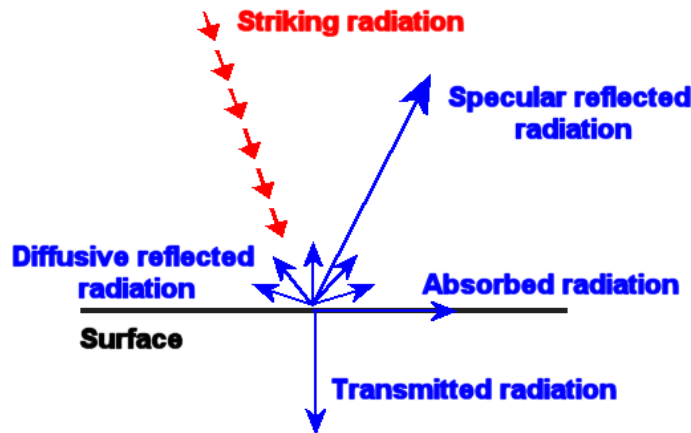**Figure 1. Spectra of an optical filter.**

Figure 2. Conceptual subdivision of the radiation striking a surface.

For a give surface temperature, the monochromatic emissivity, absorptance, transmissivity or diffusivity (see Figure 1) are a function of the wavelength only. Therefore, the amount of heat power which is exchanged or received by the elements of the system can be calculated on the bases of the wavelength of the incoming/outcoming radiation and of the surface temperature.

In most thermal software, including ESATAN-TMS, the wavelength dependency of the thermo-optical properties is reduced to the definition of only two different sets: one for the solar-UV waveband and one other for the IR waveband. No dependency upon the temperature of the surfaces is usually taken into account. In these software, the set of thermo-optical properties in the solar waveband is used to calculate the environmental fluxes coming from the Sun (direct solar flux and albedo); the latter set is used both for the calculation of the IR planetary environmental fluxes and for the internal radiative coupling.

This paper presents a set of solutions to overcome these limitations using ESATAN-TMS, implementing temperature dependant thermo-optical properties for the calculation of the radiative coupling and of the environmental fluxes. The implementation of dynamic optical properties permits also the simulation of coating whose properties vary on the base of different physical quantities or which are actively user-controlled, such as smart coatings.

3
American Institute of Aeronautics and Astronautics

Possible applications of these methods are missions in which the spacecraft is subjected to environmental radiation from sources with a broad range of temperatures, missions in which some components experience a significantly variable temperature and in general when coatings, for which the temperature dependency of the thermo optical properties can not be neglected, are used. Typical examples consist in solar orbiters or mission towards the inner planets of the solar system, radiators, filters and optical devices, cryogenic systems and smart coatings.

A. Radiative coupling

The radiative heat exchange in the thermal model is implemented using the Radiative Exchange Factors (REFs or GRs) or the view factor (GVs). The radiative heat flux between the element i and the element j may be expressed by the formula[1]:

$$q_{i,j} = \sigma \cdot \varepsilon_i \cdot \alpha_j \cdot A_i \cdot GV_{i,j} \cdot \left(T_i^4 - T_j^4\right) = \sigma \cdot GR_{i,j} \cdot \left(T_i^4 - T_j^4\right) \tag{1}$$

And therefore:

$$GR_{i,j} = \varepsilon_i \cdot \alpha_j \cdot A_i \cdot GV_{i,j} \tag{2}$$

Where σ is the Stefan-Boltzmann constant, ε_i is the emissivity of element i, α_j is the absorptivity of element j, A_i the radiating surface of element i, $GV_{i,j}$ the view factor between the elements i and j. These elements are considered one-dimensional; i.e., eq. 1 provides the integrated flux exchanged between the two elements and not for the spatial distribution of the flux on the element's surface. If the procedure used to calculate the REFs is adequate, both diffusive and specular reflections may be modeled and simulated using eq. 1.

Eq. 3 and eq. 4 express the Kirchhoff's Law, under the hypotheses of incident radiation with equal intensity from all angles and with a spectral distribution proportional to that of a blackbody at the temperature of the surface[2]. Eq. 5 is an expression of the Reciprocity Theorem[1].

$$\varepsilon_i = \alpha_i \tag{3}$$

$$\varepsilon_j = \alpha_j \tag{4}$$

$$A_i \cdot GV_{i,j} = A_j \cdot GV_{j,i} \tag{5}$$

It is therefore possible to demonstrate:

$$GR_{i,j} = GR_{j,i} \quad \Rightarrow \quad q_{i,j} = -q_{j,i} \tag{6}$$

In the thermal model, it is possible to implement the radiative conductances on the base of the view factors (eq. 2), of the current optical properties and of the radiative area, which is normally exported by the radiative solver. The base idea is to perform only one radiative analysis to calculate the view factors, and to dynamically assign the radiative exchange factors in the thermal code using eq. 2. Since the computational time of the radiative analysis is usually significantly greater than the time required to execute the thermal model, in this way it is possible to drastically reduce the computational time due to the use of variable optical properties. The thermo-optical properties depend on the surface temperature, hence the GR values should be updated for each iteration of the thermal solver and, for transient analyses, for each time step of the simulation. The emissivity (or absorptivity) value at each iteration can be calculated interpolating the tabulated relation between temperature and thermo-optical properties previously implemented.

It may be noted that, in the thermal network, the only real variable thermo-optical property is the IR emissivity or equivalently the IR absorptivity (see eq. 3). A couple of important remarks should be done:
-   It is not possible to modify the specular / diffuse reflectivity ratio. Indeed, modifying only the emissivity, it is

possible to indirectly modify the total reflectivity parameter, but the ratio of energy reflected specularly vs. the energy reflected diffusively is determined only by the view factor GV, which is usually stochastically calculated using a ray tracing method. The ray tracing method produces different results if the specular / diffuse reflectivity ratio is changed. For this reason, the GVs cannot be considered purely geometrical parameters.

- In the same way, it is not possible to modify the transmissivity of any surface. This may be easily understood considering the following example: a sequence of one body, modeled using only one node, a semi-transparent body (a filter), and another single node body. Since the transmissivity of the semi-transparent surface is greater than zero, the ray-tracing method will provide for an equivalent GV between the first and the last node. Deciding to modify the thermo-optical properties of the filter so that to have a nonexistent transmission, and keeping the same value of emissivity in order to change only the reflectivity, the software will still provide for a radiative conductor, which will be based only upon the emissivity of the radiating surface and of the absorbing surface, but not upon the transmissivity of the filter.

In order to avoid these problems, different radiative analyses varying the thermo-optical properties should be performed. After each radiative calculation, the thermal network should be solved and the resulting temperatures should be used to calculate the new set of thermo-optical properties. This process should be iterated till the desired convergence, often requiring an extremely long computational time. Fortunately, for many space applications the ratio of specular and diffuse reflectivity can be assumed constant over a wide range of temperatures, or even irrelevant to the final solution. In the same way, transparent surfaces are not very common and often their transmissivity may be considered constant over a wide range of temperatures.

B. Environmental fluxes

The direct solar flux and the albedo flux are originated from the Sun, which surface temperature can be considered constant over time. Therefore, the wavelength dependency of the thermo-optical properties can be neglected for these heat fluxes. In this section, only the planetary IR fluxes, which are originate by bodies which surface temperature may vary over a wide range, are considered. Two different aspects should be taken into account:

- the different behavior of the optical surfaces with respect to different wavelengths of the environmental radiation
- the modification of the thermo-optical properties with the variation of the surface temperature of the receiving body

The first aspect implies that, even if the system is kept at a constant temperature, its optical properties and the consequent heat load absorption may vary with the waveband of the environmental radiation (and then with the temperature of its source).

The thermo-optical properties of any optical surface should then be "weighted" upon the spectrum of the planetary radiation, which depends on the surface temperature. If the planetary radiation can be approximated as a black body radiation, then the Planck's law (eq. 7) can be used to calculate the intensity of radiation. If this assumption is not valid, the intensity of the planetary radiation is calculated multiplying the black body radiation for the emissivity spectrum of the planet.

$$I(\lambda,T)d\lambda = \left(\frac{2 \cdot h \cdot \lambda^3}{c^2}\right) \cdot \left(e^{\frac{h \cdot \lambda}{k \cdot T}} - 1\right)^{-1} d\lambda \qquad (7)$$

$I(\lambda,T)$ is the intensity of the radiation in the wavelength range between λ and $d\lambda$, λ is the wavelength of radiation, T the temperature of the black body, h the Planck constant, c the speed of light in vacuum, e the Euler's number, k the Boltzmann constant. A representation of this equation is depicted in Figure 3.
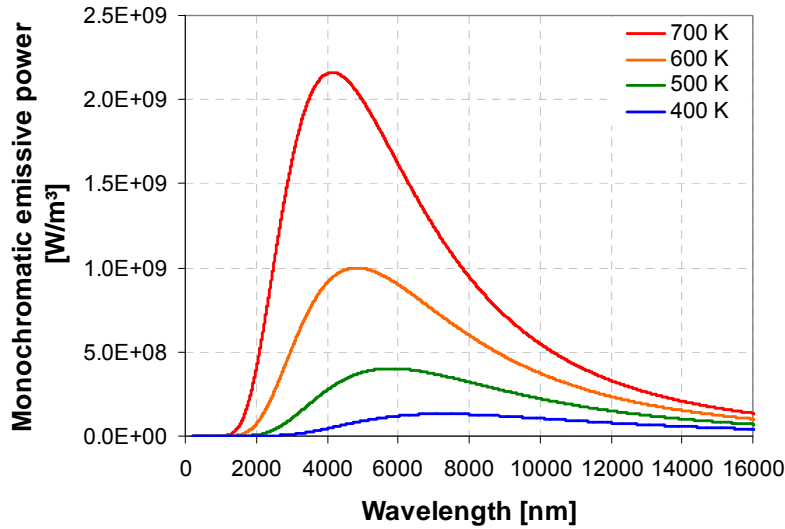
Figure 3. Black body emission spectrum for different temperatures.

As can be noted from eq. 7, the intensity of the radiation at the desired wavelength depends only on the temperature of the emitting source. But the surface temperature of a planet cannot usually be considered homogeneous. Therefore, an equivalent temperature, used to generate the radiation spectrum, should be defined and calculated. A possible solution consists in using the equivalent homogeneous temperature that the planet should have to cause the same density of power of the actual environmental radiation. This last parameter can be analytically calculated, or, for complex problems, it can be numerically determined performing a simulation with the real geometry and every surface set as black body. Thus, it is possible to express the calculated radiation power as:

$$QE = \sigma \cdot \varepsilon_{PLANET} \cdot \alpha_{BODY} \cdot GV_{PLANET-BODY} \cdot T_{EQ}^4 \qquad (8)$$

Where QE is the planetary heat power absorbed by the body, ε_{PLANET} the hemispherical total IR emissivity of the planet, α_{BODY} the total IR absorptivity of the body, $GV_{PLANET-BODY}$ the view factor between the planet and the body, and T_{EQ} the unknown equivalent temperature of the radiative source. Both the heat power and the view factor can be calculated, analytically or numerically; the absorptivity of the body is 1, if a black body has been implemented, in any case it is known; the emissivity of the planet is taken from the applied model: hence, it is possible to calculate T_{EQ}. This represents the equivalent temperature, for each orbital position and for each attitude of interest, which should be used to calculate the emission spectrum of the planet using eq. 7. The emission spectrum characteristic of each of these conditions is used to weight the thermo-optical properties spectrum of any desired surface, using the formula:

$$\eta\left(T_{EQ}, T_{BODY}\right) = \frac{\int_0^\infty I\left(\lambda, T_{EQ}\right) \cdot \eta\left(\lambda, T_{BODY}\right) d\lambda}{\int_0^\infty I\left(\lambda, T_{EQ}\right) d\lambda} \qquad (9)$$

Where η represents any thermo-optical property: emissivity, transmissivity and so on. The equation above allows the calculation of the optical parameters that should be used for the computation of the environmental fluxes, as a function of the planet equivalent temperature (see eq. 8) and of the receiving body's temperature.

The presence of the body's temperature in eq. 9 requires the solution of the thermal network, which is not necessary for the pure radiative analysis. Therefore, some iterations using the radiative solver and the thermal solver are required. A long computational time is expected following this method. Furthermore, the variation of the spectrum upon the body's temperature is often unknown, compromising the possibility of using eq. 9.

Fortunately, for a large class of materials the variation of the spectrum upon the temperature is not very sharp. The expected temperature range for a spacecraft is also much narrower than the temperature variation of most

American Institute of Aeronautics and Astronautics

radiation sources (especially for the inner planets), reducing the influence of the T_{BODY} in comparison to the T_{EQ} in eq. 9. Neglecting the influence of the surface temperature, that is considering the thermo-optical properties constant upon the body's temperature, it is possible to write:

$$\eta(T_{EQ}) = \frac{\int_0^\infty I(\lambda, T_{EQ}) \cdot \eta(\lambda) \, d\lambda}{\int_0^\infty I(\lambda, T_{EQ}) \, d\lambda} \tag{10}$$

Summarizing it is possible, for each orbital position and attitude of interest, to calculate the planet's equivalent temperature. If the optical spectrum of the body is known, this curve can be weighted on the planet's radiation spectrum (not necessarily a black body radiation) and integrated on the relevant waveband in order to calculate the total hemispherical optical properties to be implemented for the calculation of the planetary heat radiation.

This procedure involves the use of the radiative solver only. If the dependency of the thermo-optical properties on the body's temperature is not negligible, some iterations using the thermal solver are unavoidable.

II. Complex 3D geometries

Space systems make commonly use of complex 3D geometries: antennas, reflective baffles, optical devices are all system that are difficult to integrate in a thermal geometrical model.

Often the shape cannot be approximated beyond a defined limit, and these elements must be represented using a large number of shells, with an elevated modeling and computational time costs. Optical devices require particular modeling care, since small shape variations may strongly affect their functioning and produce unrealistic simulation results. For instance, the amount of environmental radiation rejected by reflective baffles depends upon the shape of its optical surfaces.

This condition can be better understood considering that some optical surfaces are specifically designed to direct the radiative flux towards a specific target. For instance, some antennas are used to focus the radiation on a small component, which therefore experiences a high heat load. Small variations of the geometry or too coarse approximations of the shape can modify the optical path and strongly reduce the heat load on the target surface. Similarly, some reflective surfaces may be designed to reflect the striking radiation through a small aperture, in order to minimize the heat absorption and the clear aperture of the system.

Currently ESATAN-TMS can model conical surfaces, paraboloids and spheroids: other complex geometries commonly used in space applications, like ellipsoids, hyperboloids and generic surfaces of revolution are not yet available. It is therefore necessary to approximate the desired shape using the three base shells mentioned above. The goal of the optimal discretization is to identify the minimal number and the type of shells to be used, together with their mesh, in order to achieve the desired accuracy.

Different criteria can be used to assess the efficiency of a discretization, which can be assigned to one of two distinct categories:

- pure geometrical parameters
- radiative parameters

Figure 4. Geometrical error.

The first class includes the area between the desired curve section and the approximated one (see Figure 4), and the integral of the angle from a reference to the normal to the surface (compared between the ideal and approximated curve).

The second category consists in comparing the environmental fluxes calculated analytically (on the ideal geometry) and numerically (on the approximated geometry).

The geometrical parameters are used to define a first approximated geometry and its discretization. The radiative parameters can be used to iteratively optimize the geometrical model.
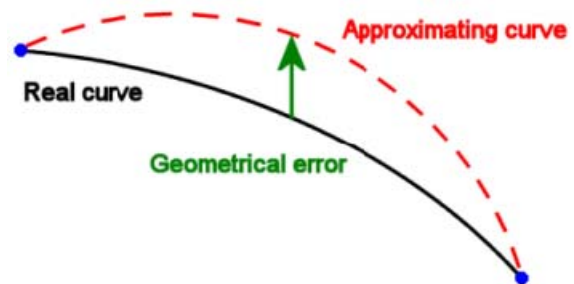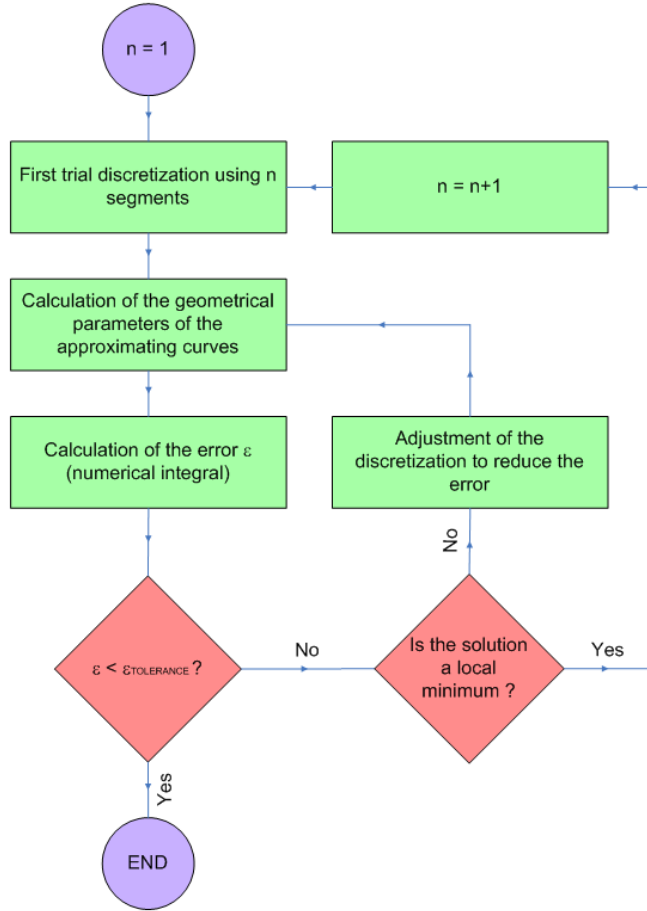
Figure 5. Discretization flow chart.

In Figure 5 the logical path of the process is depicted. As a first attempt, it is possible to try to model the desired surface using only one shell. The error parameter (in whatsoever way it has been defined) is calculated, and then this value is compared with the maximal allowable error. If the calculated value is the greatest, the process should be iterated trying with two shells, and so on till the achievement of the desired accuracy.

Considering only surfaces of revolution, it is possible to analyze the approximation problem in two dimensions, analyzing the generatrix of the surface. We define $F(x,y)=0$ as the 2-dimensional function of the generatrix of the reference surface ($y = f(x)$ in explicit format) and $\Phi(x,y)= 0$ as the function of the generatrix of the approximating surface ($y = \Psi(x)$ in explicit format).

The function Ψ depends on the type of the chosen approximating surface: Straight lines (eq. 11) for cones, parabolas (eq. 12) for paraboloids and circumferences (eq. 13) for spheres:

$$\Phi_{LINE}(x, y) = a \cdot x - y + b = 0 \tag{11}$$

$$\Phi_{PAR}(x, y) = a \cdot y^2 + b \cdot y - x + c = 0 \tag{12}$$

$$\Phi_{CIRC}(x, y) = (x - a)^2 + (y - b)^2 - r^2 = 0 \tag{13}$$

The equations of the parabola and of the circumference can be further approximated. In order to represent surfaces of revolution, which cross section is a circle, it is necessary to impose that the vertex of the parabola and the center of the circumference lie on the axis of rotation. If this condition is not applied, the produced 3D results show asymmetries in tangential direction. This constraint translates into a relation between the geometrical parameters of the curve, which eliminates the parameter b from eq. 12 and eq. 13:

American Institute of Aeronautics and Astronautics

$$y_{LINE} = \Psi_{LINE}(x) = a \cdot x + b \tag{14}$$

$$y_{PAR} = \Psi_{PAR}(x) = \left(\frac{x-c}{a}\right)^{\frac{1}{2}} \tag{15}$$

$$y_{CIRC} = \Psi_{CIRC}(x) = \left[r^2 - (x-a)^2\right]^{\frac{1}{2}} \tag{16}$$

The functions describing the three presented generatrixes depend upon two geometrical parameters. A unique curve can be set constraining the approximating generatrix to cross the reference generatrix on two points

Defining the approximation error as the difference between the approximated and the reference generatrixes:

$$\xi(x) = \Psi(x) - f(x) \tag{17}$$

$$\xi = \int_0^l |\Psi(x) - f(x)| \, dx \tag{18}$$

Where $\xi(x)$ is the local error, ξ is the total error, $f(x)$ the reference generatrix, $\Psi(x)$ the approximated curve and l its length along the axis of rotation (assumed x without affecting generality). It is therefore possible to write:

$$\xi = \sum_{i=1}^{n} \left\{ \int_{x_{i-1}}^{x_i} |\psi_i(x) - f(x)| \, dx \right\} \tag{19}$$

$$0 = x_0 < x_1 < x_2 < \ldots < x_{n-1} < x_n = l \tag{20}$$

where ψ_i is the local approximation (arc of circumference or parabolic segment) of the real curve, and n is the number of segments in which the real surface has been divided. The local approximation is function only of the axial coordinate x. Eq. 19 is function of only $n-1$ parameters: the x-coordinates of the start and end points of the discretization segments ($x_1, \ldots, x_{n-1}$).

The number of approximating surfaces n is usually constrained by computational limits.

To find the optimal approximation for a given n, eq. 19 should be minimized with respect to the x_i parameters which allow achieving the optimal approximation.

A reasonable simplification consists in defining a maximal acceptable error $\xi < \xi_{MAX}$ and proceeding iteratively selecting different set of approximating segments until the required maximal error is met. Doing that, all the approximating curves are univocally identified but no absolute minimization is guaranteed. The geometrical parameters of the approximating curves can be independently determined for each single segment, requiring that the approximating curve intersects the real curve at the beginning and at the end of its domain:

$$\forall i = 1, \ldots, n \qquad \begin{cases} \psi_i(x_{i-1}) = f(x_{i-1}) \\ \psi_i(x_i) = f(x_i) \end{cases} \tag{21}$$

This allows calculating the two geometrical parameters that constrain the approximating curve (see eq. 14, eq. 15 and eq. 16).

The first simplest solution consists in adopting a homogeneous discretization along the x axis. Thickening the mesh by the steepest parts of the curve, it is possible to reduce the approximation error. It is possible to iterate the process: an initial mesh can be defined, the system of eq. 21 solved and the single errors for each segment of discretization calculated. Then, the elements which show the largest errors may be corrected reducing their domain in x, and increasing the width of the segments which instead present the lowest errors.

9

American Institute of Aeronautics and Astronautics

III. Standard thermal analysis procedure

The thermal analysis of a model design generally adheres to the following pattern: starting with the full description of the model configuration, the engineer makes an idealized (simplified) geometric model expressed in terms of the primitive types (i.e. building blocks). To this geometric model is added information about the thermo-optical properties of the materials used in the construction of the model. This geometric model is then discretised in some way to permit the formulation of a set of discrete (coupled) equations in place of the continuous differential equations describing the transport of heat within the model. The coefficients of this set of equations will generally involve heat capacities and conductivities of the materials of the model, heat sources and sinks, external heat inputs and losses, and radiative exchanges inside and outside the model. All of these coefficients must be computed to complete the thermal mathematical description of the model. Once the coefficients are available, the set of equations may be solved, possibly with a time or other dependence of some of the terms, to enable a simulation of the model and its environment to be made.

The results from the simulation are examined and compared with design criteria, test results, other simulations, etc.; the model is modified as necessary to correct errors and to reflect changes in design; and a further simulation is carried out. This cycle continues until satisfactory predictions are obtained for the range of environmental conditions that the model will experience.

Figure 6. Thermal modeling cycle.

ESATAN-TMS Workbench is a widely used 3D surface-modeling environment, allowing the user to perform the type of thermal analysis as described above.

The standard procedure to perform a complete thermal analysis using ESATAN-TMS is

- Creation of the Geometrical Mathematical Model (GMM), based upon the use of complex geometries from predefined primitive shapes (quadrilaterals, discs, cones, spheres, boxes, etc). These primitives will be assembled using Boolean operations, including cutting. The user can associate them with material properties (density, heat specific and conductivity) and thermo-optical properties (IR or UV properties).
- A radiative mesh is applied to the geometry and an enhanced Monte-Carlo ray-tracing algorithm coupled with automatic accuracy control is used to calculate radiative coupling between the mesh faces and to derive environmental fluxes (solar, planet and albedo). In support of using different mesh densities for the radiative solution and the thermal solution, a thermal mesh can be overlaid on the radiative mesh with Workbench automatically performing the mapping operation.
- Computation of the conductive couplings between adjacent nodes within Workbench using the "Far-Field" Method[3].
- Definition of all the boundary conditions applicable to the model. Workbench provides an interactive and easy way to define efficiently time and temperature dependant boundary conditions.
- Through the use of a case control facility, Workbench will automatically generate the Thermal Mathematical Model (for ESATAN or SINDA/G solver) containing the calculated view factors, radiative exchange factors, conductive couplings, environmental fluxes and boundary conditions.
- The generated TMM will be automatically run using ESATAN-TMS Thermal module. The calculated temperatures will be available for being post-processed, either inside Workbench by applying them onto the geometrical model, or inside ThermNV, ESATAN-TMS post-processing tool.

A couple of remarks can be made.

In the generation of the TMM, some information of the GMM is lost. In the lumped parameters model indeed, all the data about the geometry of the surfaces are condensed in a list of areas and view factors (or radiative exchange factors). In the same way, no information about the specular / diffuse reflectivity or about the transmissivity of the surfaces are still available: only the emissivity / absorptivity is reported in the definitions of the nodes. Again, all the parameters of the orbit are not available in the TMM, in which all these information are reduced to a list of environmental fluxes. For all these reasons, it is not possible to perform another complete radiative analysis from the thermal model, but it is necessary to modify the GMM.

It is important to remark that this is not a limitation of the software, but it is an intrinsic problem of the lumped parameters method. This simple but useful instrument for the solution of the thermal problem compresses all the information concerning a real element into a single node (and thus the "lumped parameters" name). Each node has the following properties: temperature, thermal capacitance, radiative area, IR emissivity and UV absorptivity. It is also possible to implement user defined parameters, but not to recover all the information about the geometry which are necessary to perform a radiative analysis.

Summarizing, if the lumped parameters method is applied, the radiative problem is conceptually decoupled from the thermal problem. The radiative problem is usually solved first to provide for the inputs for the thermal problem, such as radiative exchange factors and environmental fluxes, when the results of the thermal problem (in particular the temperatures) are not yet known. If the dependency of the radiative results from the temperatures is not negligible, the only way to properly take into account for this relation is to iterate the solution of the GMM and of the TMM. This necessity is due to the mathematical representation of the problem, and not to software limitations.

IV. Implementation of variable thermo-optical properties

A. Internal fluxes and radiation towards deep space

1. Description

The first and simplest case is the implementation of temperature-dependant thermo-optical properties for the calculation of internal radiation (radiative heat exchange between elements of the system) or for the calculation of the radiation towards the deep space (radiative heat exchange with a radiative sink).

In this section, the dependency of the thermo-optical properties upon the temperature is supposed to be explicitly known: that is, the relation between temperature and absorptivity, emissivity, reflectivity and transmissivity can be tabulated. An example is shown in Figure 7. For a method to determine the explicit relation from the optical spectrum, see §I-B.

It is necessary to perform the radiative analysis just once, using any coating: the desired output is the list of the view factors (GVs). These are (theoretically) purely geometrical parameter, which do not depend on the surfaces coatings or on their optical properties.

Figure 7. Explicit relation between temperature and thermo-optical properties.

2. Procedure using ESATAN-TMS

The following procedure should be applied to the analysis file. It is not possible to perform the following operations using only the ESATAN-TMS Graphical User Interface (GUI).

From the analysis case within Workbench, it is possible to automatically create the analysis file (input file for the ESATAN solvers). In this analysis file, it is possible to output the calculated view factors (GVs) that will automatically be reported in the $CONDUCTORS block as described below:
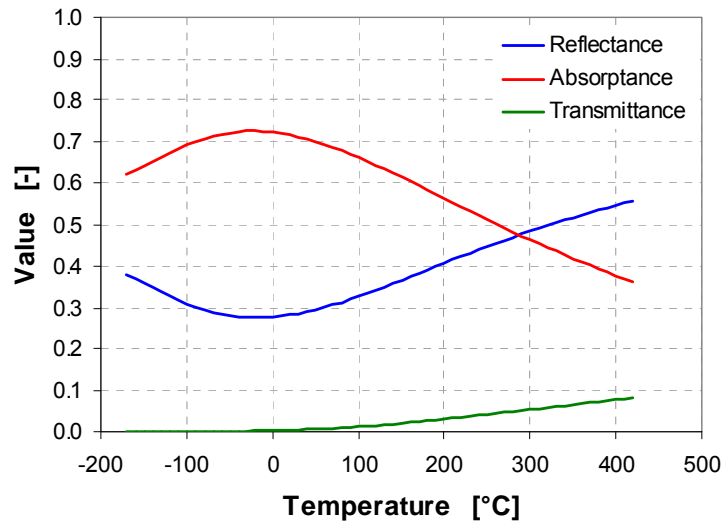
```
$CONDUCTORS

   GV(1001, 1002) = 0.07623;
   GV(1001, 1003) = 0.02112;
   GV(1001, 1004) = 0.10061;
   GV(1002, 1003) = 0.05439;
   GV(1002, 1004) = 0.06667;
   ...
```

The following step is to define in the $ARRAY block the temperature dependency of the emissivity. This can then be used in the interpolation routine INTERP which will be called at each time step. The VFAC routine is used to update the GRs values on the base of the GVs and of the interpolated emissivities.

```
$CONSTANTS

   $ARRAYS
      $REAL

         TI_TEMPERATURES(5) = -50.0, 0.0, 20.0, 50.0, 100.0;
         TI_EMISSIVITY(5) = 0.567884, 0.487767, 0.291115, 0.203785, 0.151202;

   ...

$VARIABLES1

   WHILE (iNode .LE. NNodes)
      EPS:1000(iNode) = INTERP(T:1000(iNode), TI_TEMPERATURES, TI_EMISSIVITY, 1)
      iNode = iNode + 1
   ENDWHILE

   CALL VFAC
```

3. Example 1

The first example illustrated consists of a sphere with a diameter of 100 mm, surrounded by a cubic shroud which side length is 300 mm. The shroud surfaces are assumed to be perfect black bodies, whereas the sphere is made of titanium. In Figure 8 it is possible to see the measured emissivity of a titanium sample vs. temperature. The sample has been subjected to mechanical and thermal finishing.

The black body shroud has been set as radiative sink with a fixed temperature of -20 °C, which is also the initial temperature of the sphere. A linearly variable dissipation power has been applied to the sphere, starting from 0 W at the beginning of the simulation till 100 W after 100 s. The results in terms of sphere temperature are reported in Figure 9.

As can be seen, the results obtained implementing temperature-dependant thermo-optical properties significantly differ from the results using constant

Figure 8. IR emissivity/absorptivity of a titanium sample vs. temperature.

optical properties. In particular, implementing the emissivity corresponding to -20 °C, which is the initial temperature, the difference after 100 s is more than 60 °C. Using an emissivity corresponding to an expected average value, for instance the value corresponding to 30 °C, the difference is still high (57 °C). The blue curve in Figure 9 instead represents the temperature evolution of the sphere implementing a constant emissivity corresponding to 290 °C. This value has been numerically calculated so that the final temperature is equal to the final temperature adopting the variable thermo-optical properties. Although the final temperatures coincide, the temperature profile of the case with fixed emissivity is significantly higher than the profile of the case which makes use of variable emissivity, especially in the central area of the chart. Therefore, even this last case can be considered representative of only one single point. Most important, there is no way to calculate a priori the required emissivity in order to match the real results at a specific time step. This value should be numerically calculated after a simulation in which the temperature-dependency of emissivity has been taken into account.

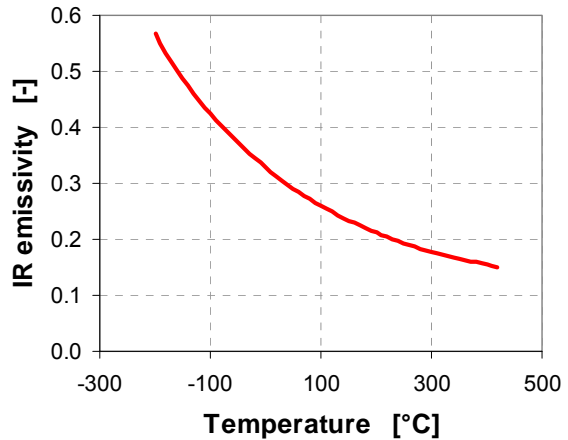The values of IR emissivity during the simulation are reported in Figure 10.
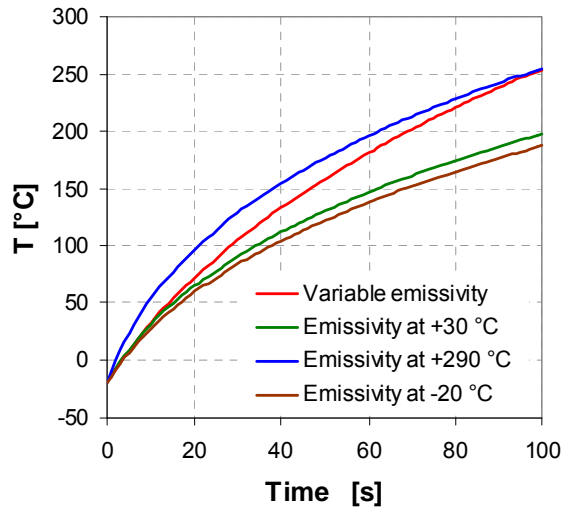
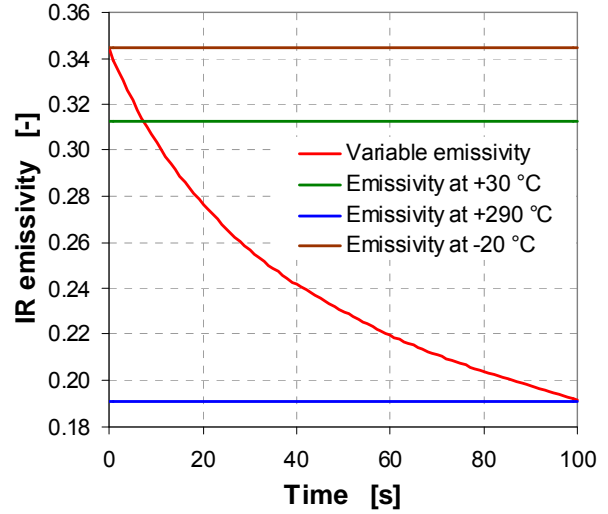**Figure 9. Sphere temperature vs. time.**

Figure 10. IR emissivity of the sphere vs. time.

B. Environmental fluxes

1. Description

The calculation of the environmental heat fluxes, and in particular of the planetary IR fluxes, represents an increment of the complexity with respect to the previous case.
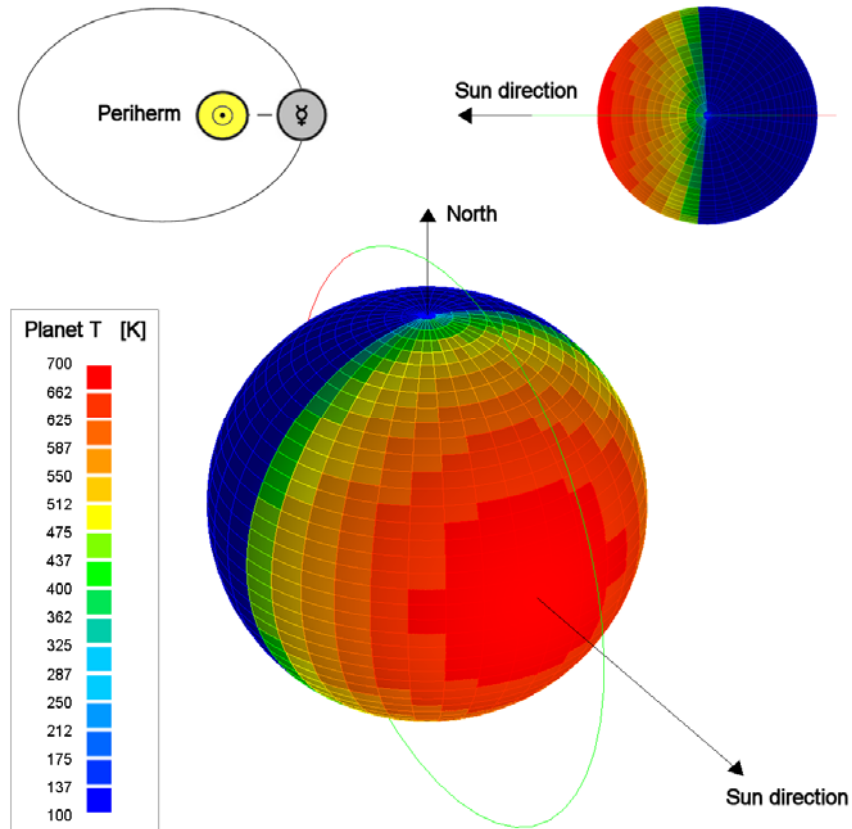

Figure 11. The orbit of the example.

A good example is represented by the planet Mercury, which is the case for which this method has been developed. The night side of the planet experiences temperatures down to 100 K[4], whereas the subsolar point at perihelion reaches 680 K[5]. This causes a strong variation of the radiation intensity but also a variation of the radiation waveband. A noon/midnight polar orbit when Mercury is at the perihelion presents the extreme

Parameter	Value	
Mercury true anomaly	0.0	deg
Sun-planet distance	$4.60011 \cdot 10^7$	km
Right ascension of ascending node (Ω)	180.0	deg
Orbit Inclination (i)	90.0	deg
Argument of Periherm (α)	16.0	deg
Altitude of Periherm	400.0	km
Altitude of Apoherm	1508.0	km

Table 1. Parameters of the example orbit.

temperature variations which have been introduced. An illustrative orbit of this type, used in the following examples, is depicted in Figure 11; its main parameters are listed in Table 1.

Before implementing the temperature dependency of the thermo-optical properties, the equivalent planet's temperature (see eq. 8) should be calculated. The planet's temperature must be modeled using the same temperature map that will be used for the real model. Then, a simple dummy model can be used to calculate the planetary radiation. A possible solution is the use of a black body disc, which size and attitude should be representative of the real model. From the planetary heat flux, the equivalent planet's temperature is calculated for each time step of the simulation.

2. Procedure using ESATAN-TMS

For each step of the radiative analysis, the thermo-optical properties can be calculated using the corresponding equivalent planetary temperature (see eq. 8). The results can be stored in the ESATAN-TMS geometry file using an array of opticals.

```
STRING PropEnv[42] = {"avrg", "AA", "AB", "AC", "AD", "AE", "AF", ...

OPTICAL opt_Coating;

opt_Coating[avrg] = [0.262855, 0.737145, 0.0, 0.15, 0.0, 0.0, 0.0, 0.85];
opt_Coating[AA] =   [0.524147, 0.475853, 0.0, 0.15, 0.0, 0.0, 0.0, 0.85];
opt_Coating[AB] =   [0.479518, 0.520482, 0.0, 0.15, 0.0, 0.0, 0.0, 0.85];
opt_Coating[AC] =   [0.375622, 0.624378, 0.0, 0.15, 0.0, 0.0, 0.0, 0.85];
opt_Coating[AD] =   [0.293954, 0.706046, 0.0, 0.15, 0.0, 0.0, 0.0, 0.85];
opt_Coating[AE] =   [0.242266, 0.757734, 0.0, 0.15, 0.0, 0.0, 0.0, 0.85];
opt_Coating[AF] =   [0.310253, 0.789747, 0.0, 0.15, 0.0, 0.0, 0.0, 0.85];
...
```

The optical arrays have been defined following the ESARAD convention: IR emissivity, IR diffusive reflectivity, IR transmissivity, UV absorptivity, UV diffusive reflectivity, UV transmissivity, IR specular reflectivity, UV specular reflectivity. It can be noted that only the thermo-optical properties in the IR waveband have been changed: since the solar superficial temperature can be considered constant, there is no need to modify the optical properties in the solar-UV waveband.

For each step of calculation, it is necessary to update the thermo-optical properties set. This can be done modifying the normal kernel file, which contains all the instructions for the radiative calculation. This file can be created using the Workbench, specifying all parameters of the radiative case, of the mission and of the accuracy. Then, it can be exported, modified and re-loaded with the made modifications.

The following code shows an example of a kernel file modified to update the thermo-optical properties at each time step. The variable *CaseName* should be replaced with the name of the actual radiative case. The FOR loop repeats the radiative computation as many time as it has been specified in the radiative case definition. Before any execution of the radiative calculation, the thermo-optical properties are updated, assigning to the *PROP_ENV* variable the proper value of the *PropEnv* array, which has been previously defined in the geometry file and that returns the index of the optical array.

```
PROP_ENV = CaseName.PROP_ENV;

CALCULATE (radiative_case = CaseName,
           calc_types = "REF",
           pos_index = 1,
           eclipse_check = TRUE);

FOR (orbit_index = 1;
     orbit_index <= CaseName.NUM_ORBIT_POSITIONS;
     orbit_index = orbit_index + 1)
```

```
            CaseName.PROP_ENV = PropEnv[orbit_index + 1];
            PROP_ENV = CaseName.PROP_ENV;

            CALCULATE (radiative_case = CaseName,
                       calc_types = "SAF, PAF, ALBEDO_PAF",
                       pos_index = orbit_index,
                       eclipse_check = TRUE);

        END_FOR

        PROP_ENV = CaseName.PROP_ENV;
```

Since the radiative exchange factors have no influence on the calculation of the environmental fluxes, they can be calculated only once at the beginning of the radiative calculation. This is valid only for static geometries: for kinematic models it is necessary to recalculate the REFs for each time step. The thermo-optical properties set used for the calculation of the REFs is the first listed in the *PropEnv* variable, which corresponds to the average (*avrg*) label. This set of optical properties is representative of the temperature at which the surfaces exchange heat inside the system, which is in general different than the planet's temperature.

When the previous code is executed, ESATAN-TMS provides for warning messages, which should be ignored. Since these messages interrupts the simulation, if the kernel file is executed using the GUI, it is recommended to perform this type of operation in batch line.

3. *Example 1*

The implementation of temperature-dependant thermo-optical properties for the calculation of the environmental fluxes will be presented using the orbit around Mercury described in §IV-B-1 as example. This planet has been chosen due to its proximity to the Sun and to its peculiar orbit, which causes extreme temperature variations on the planet's surface. The Mercury's temperature is depicted in Figure 11. A simple disc has been used to assess the planetary fluxes along the orbit. The thermo-optical properties of the Ti sample reported in Figure 8 have been used. The orbit starts in the night side, 16° above the equator.

The simulation has been performed for three different set of thermo-optical properties. In the first one, the IR absorptivity has been calculated weighting the spectrum of the sample on the planetary emission spectrum, and the values have been dynamically updated during the simulation. The other two cases instead make use of single values of IR absorptivity.

The first of these is simply the arithmetical average of the absorptivity along the whole measured spectrum.

Another method consists in trying to reproduce the equivalent temperature that would cause the same total amount of environmental fluxes on the body, assuming a constant heat flux along the orbit. This condition is expressed in eq. 22:

$$\frac{\int_0^\tau \phi(t)\,dt}{\tau} \cong \frac{\sum_{i=1}^n \phi_i \cdot \Delta t_i}{\tau} = \phi^{(average)} = \sigma \cdot \varepsilon_{PLANET} \cdot \alpha_{BODY} \cdot GV_{PLANET-BODY}^{(average)} \cdot T_{EQ}^4 \qquad (22)$$

Where τ is the temporal length of the simulation (typically the orbit period), Φ is the IR flux and n is the number of steps of the simulation. Please note that the average view factor along the orbit should be used. The view factor can be easily calculated for each position numerically using ESATAN-TMS or even analytically, and then averaged upon time. Using the relation eq. 22, and implementing the orbit described above, it is possible to evaluate the equivalent temperature of Mercury as

$$T_{EQ} = \left(\frac{\sum_{i=1}^n \phi_i \cdot \Delta t_i}{\tau \cdot \sigma \cdot \varepsilon_{PLANET} \cdot \alpha_{BODY} \cdot GV_{PLANET-BODY}^{(average)}} \right)^{\frac{1}{4}} = 209.6\,°C \qquad (23)$$

The IR absorbed fluxes, for the three different cases, are plotted in Figure 12; the errors with respect to the case which makes use of temperature-dependant thermo-optical properties are reported in Figure 13.
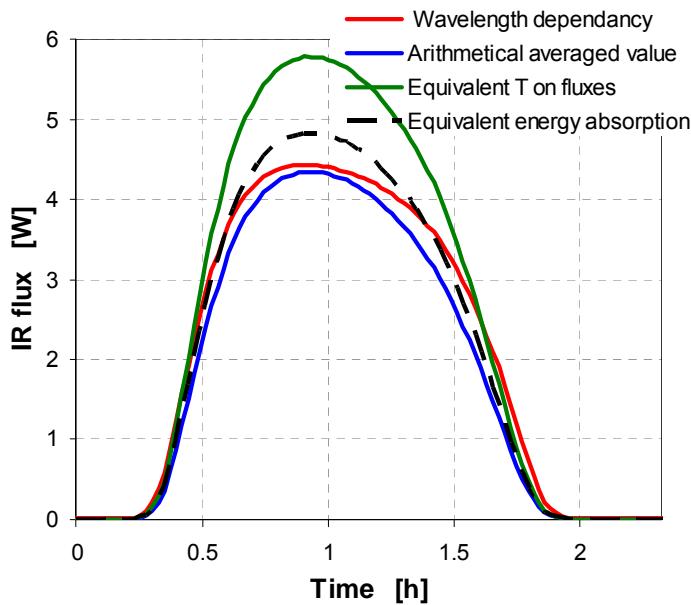
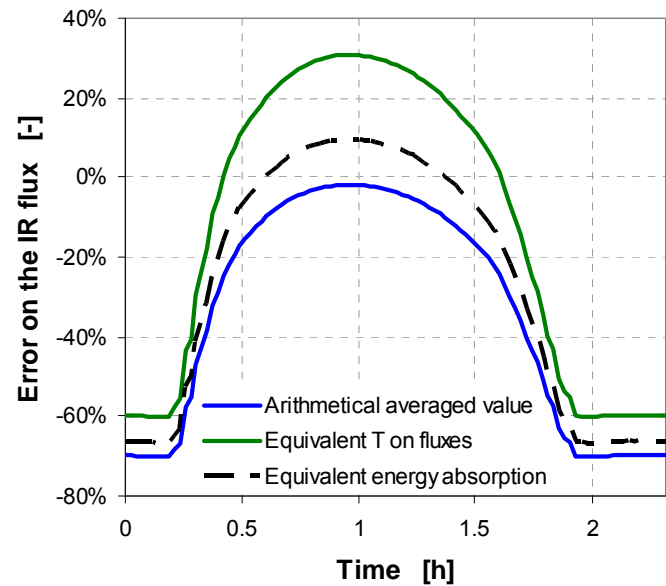**Figure 12. IR fluxes from the planet.**

Figure 13. Error on the heat flux implementing fixed thermo-optical properties.

As can be seen, the two proposed approximations are not able to reproduce the real radiative behavior. Implementing the average of the emissivity, the IR planetary flux is underestimated for each orbital position. In particular, in the night side of the planet the absolute value of the error raises up to 70 %; the total absorbed energy along one orbit is only 93 % of the real value. Implementing a fixed emissivity, based on the equivalent temperature of the planet, the planetary fluxes are underestimated in the night side and overestimated in the day side of the planet. The flux peak is overestimated by a factor of 1.3, and the total absorbed energy is 20 % more than in the real case.

The fixed emissivity which causes the same total energy absorption has been numerically calculated and is reported in Figure 12 and Figure 13 as a dashed black line. Even this solution, which is not known a priori, is not able to reproduce the real IR absorption curve, and causes an overestimation of the planetary flux peak of about 10 %.

4. Example 2

The second example presents the combined used of temperature-dependant thermo-optical properties for the calculation of the absorbed environmental fluxes and of the internal radiative exchange. Moreover, the use of active coatings will be introduced. This brand-new class of coatings promises to become a very important factor in the design of space-purposed thermal controls. Active coatings allow controlling the thermo-optical properties of special surfaces, usually by means of extremely low-power electric signals. The presented method can be used also to simulate other types of dynamic coatings, such as thermochromic materials.

The active coating used in this example is EclipseVED™, developed by Eclipse Energy Systems, Inc.[6]. EclipseVED™ is an electrochromic coating which can be controlled through a very low power (order of magnitude: 10^{-2} W·m^{-2}). This material can assume two different set of optical properties in the IR waveband: bleached, with low emissivity/absorption, and colored, which is used instead to achieve high values of IR emissivity/absorption. The spectra of the two modes of the EclipseVED™ coating are reported in Figure 14. From this data, the thermo-optical properties have been integrated over the black body radiation. The explicit dependence of IR absorptance vs. temperature has been found using the procedure described in §I-B. Since there is no data about how the material spectrum changes with its surface temperature, it has been assumed that no significant variation of the emissivity spectrum occurs with variation of the temperature. Therefore, the emissivity of the surface as a function of the surface temperature has been considered coincident with the absorptivity with respect to an incident radiation from a source with the surface temperature.
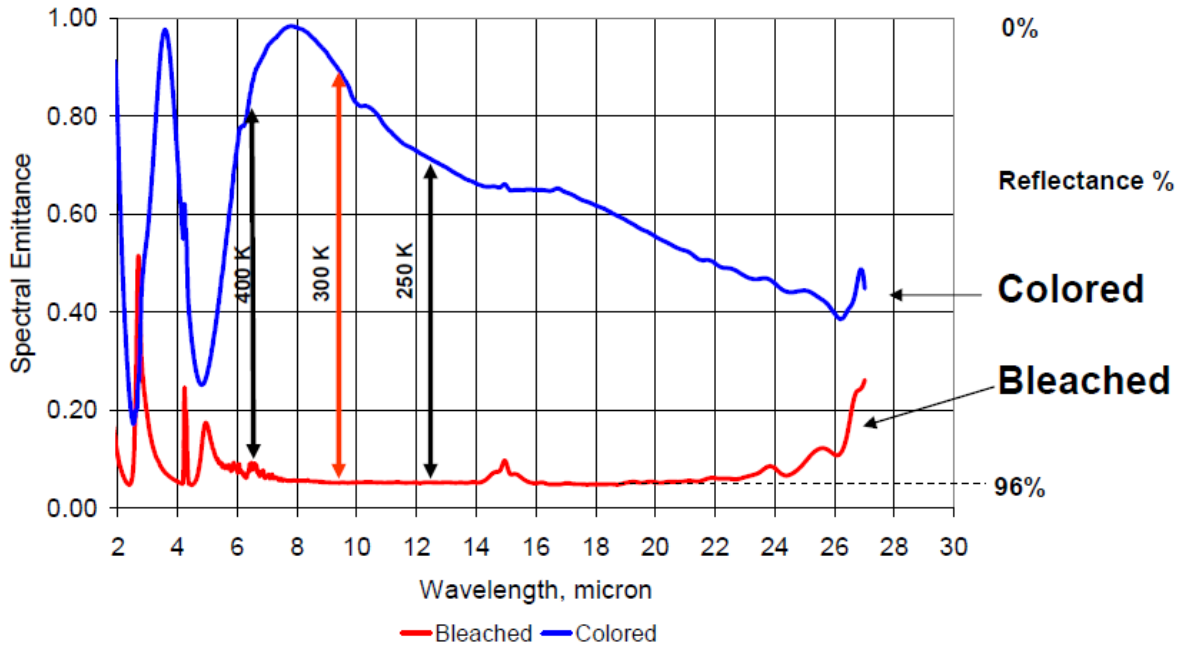
American Institute of Aeronautics and Astronautics

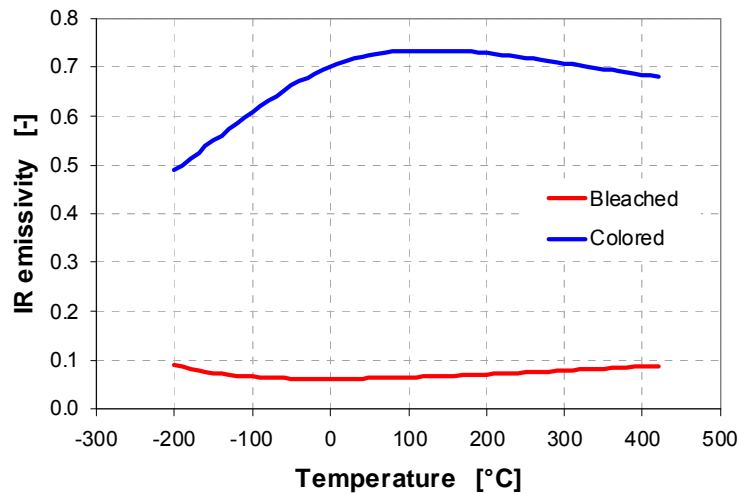**Figure 14. EclipseVED™ spectra[7].**

Figure 15. EclipseVED™ coating, dependency of emissivity upon temperature.

A complete radiative and thermal simulation has been performed implementing both modes (bleached and colored). A simple disc, always nadir-pointing, performs the orbit described in §IV-B-1. The use of a high emissivity coating, such as the colored mode of EclipseVED™, causes high energy absorption from the planet, but also low maximal temperatures. When the surface becomes hot, as a consequence of planetary and solar fluxes, a high IR emissivity allows for an efficient dissipation of the heat. On the other hand, the use of a low emissivity coating (like the bleached mode of EclipseVED™, causes low power absorption from the planet but high temperature peaks. A good solution can therefore be to implement the bleached thermo-optical properties when the disc faces the hot side of the planet, and the colored mode for the rest of the orbit. A possible switch condition may refer to the planetary heat flux received from the planet: when this value is larger than a predefined limit, the bleached mode is activated. The solution implemented in this simulation consists of switching to the bleached mode when the incident planetary flux exceeds 0.01 W·m^{-2}, and to the colored mode when the planetary flux goes below this value. Results in terms of IR fluxes and disc temperature are reported in Figure 16 and Figure 17.
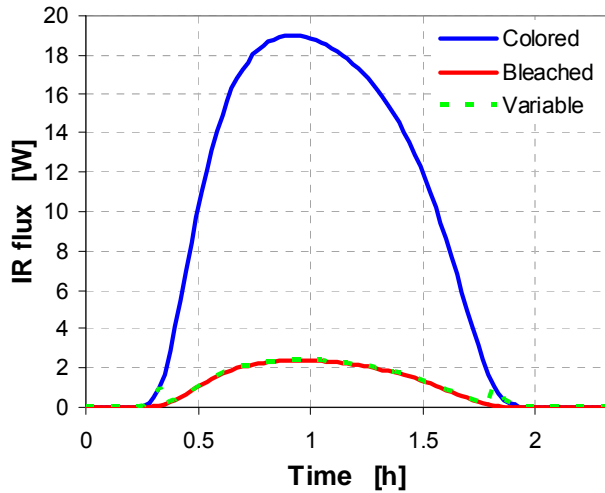
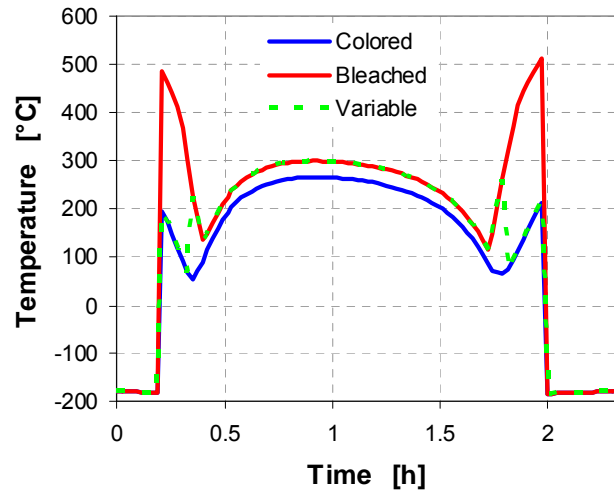Figure 16. Planetary IR fluxes absorption.

Figure 17. Disc temperature vs. time.

The temperature peaks which occur using the bleached mode for the whole orbit are due to the solar radiation. In this segment of the orbit, the planet is cold but the disc experiences a low aspect angle with respect to the Sun. Since the solar thermo-optical properties are fixed, at this point it is important to take advantage of the colored mode to re-emit as much as possible the absorbed solar radiation. Shortly later, when the planet's temperature grows hot and the Sun aspect angle decreases, a bleached mode is preferable in order to absorb less planetary fluxes (down to 12 % of the colored values). As a drawback, this causes a small increment of the surface temperature with respect to the case which makes use of the colored mode only.

It is not easy to dynamically modify the radiative analysis: switching from one set of thermo-optical properties to one other can be done only at a prearranged time step. It is not possible to switch from one condition to one other on the base of a parameter which is calculated along the simulation. Therefore, the best solution is to implement the control on the active coating in the thermal model. Two whole radiative analyses should be run, one for the bleached mode and one for the colored mode. The IR absorptivity for each time step of the simulation can be calculated from the curves reported in Figure 15 and using eq. 8 and eq. 10. Both the planetary flux and the emissivity for the two cases should be implemented in the thermal model:

```
SU1000(41) = # SOLAR ABSORBED
    0.000000, 1.231053, 0.000000, 0.000000, 0.000000, ...

AL1000(41) = # ALBEDO ABSORBED
    0.000000, 0.051917, 0.163045, 0.309949, 0.714186, ...

PL1000_BLACKBODY(41) = # PLANET ABSORBED (BLACK BODY)
    0.025496, 1.913371, 5.964851, 11.325100, 26.078820, ...

PL1000_COLORED(41) = # PLANET ABSORBED (COLORED MODE)
    0.013316, 1.377715, 4.374247, 8.179911, 17.990770, ...

PL1000_BLEACHED(41) = # PLANET ABSORBED (BLEACHED MODE)
    0.001992, 0.118157, 0.397461, 0.814742, 2.175783, ...

EPS_COLORED(41) = # IR EMISSIVITY (COLORED MODE)
    0.52228339, 0.72004565, 0.73333716, 0.72228157, 0.68986133, ...

EPS_BLEACHED(41) = # IR EMISSIVITY (BLEACHED MODE)
    0.07813240, 0.06175352, 0.06663381, 0.07194126, 0.08343103, ...
```

The standard routine used for the interpolation of the environmental fluxes should be modified, introducing an IF structure which discriminates between two different cases modifying the implementation of the planetary flux:

```
SUBROUTINE QCYCLC LANG = MORTRAN
    QS1000 = INTCYC (TIMEM, ORBTIM, SU1000, 1, PERIOD, 0.0D0)
    QA1000 = INTCYC (TIMEM, ORBTIM, AL1000, 1, PERIOD, 0.0D0)
    #
    IF (INTCYC (TIMEM, ORBTIM, PL1000_BLACKBODY, 1, PERIOD, 0.0D0) .GT. (0.01 / A1000)) THEN
        QE1000 = INTCYC (TIMEM, ORBTIM, PL1000_BLEACHED, 1, PERIOD, 0.0D0)
    ELSE
        QE1000 = INTCYC (TIMEM, ORBTIM, PL1000_COLORED, 1, PERIOD, 0.0D0)
    END IF
    #
RETURN
END
```

Finally, the emissivity of the interested surfaces should be updated considering the proper surface temperature, and the GRs updated for each time step and for each iteration of the thermal solver. The radiative analysis should provide for the necessary view factors (the radiative exchange factors are calculated using the VFAC subroutine).

```
$VARIABLES1

    IF (SOLVER(:2) .EQ. 'SS') THEN
        CALL QAVERG
    ELSE
        CALL QCYCLC
        CALL RCYCLC
    END IF

    IF (INTCYC(TIMEM, ORBTIM, PL1000_BLACKBODY, 1, PERIOD, 0.0D0) .GT. (0.01 / A1000)) THEN
        EPS1000 = INTCYC (TIMEM, ORBTIM, EPS_BLEACHED, 1, PERIOD, 0.0D0)
    ELSE
        EPS1000 = INTCYC (TIMEM, ORBTIM, EPS_COLORED, 1, PERIOD, 0.0D0)
    END IF

    CALL VFAC
```

V.   Approximation of 3D geometries

A. Code
The best way to implement a large number of shells makes use of the FOR DO loop. Inside the loop, it is possible to call a shell generator command varying the parameters for each iteration. If the relevant parameters are stored in matrixes, it is possible to refer to the proper values using the FOR DO loop index.

The geometrical shells can be defined using parameters or points: in this paper, the latter solution will be presented. The first step is the identification of the relevant points: since a numerical code is the best solution to calculate the geometrical parameters of eq. 14, eq. 15 and eq. 16 for a large number of shells, and in case to numerically calculate the minimum of the error (eq. 19), the same code can be used also to calculate the position of the definition points. An example of the definition points for the sphere is shown in Figure 18.
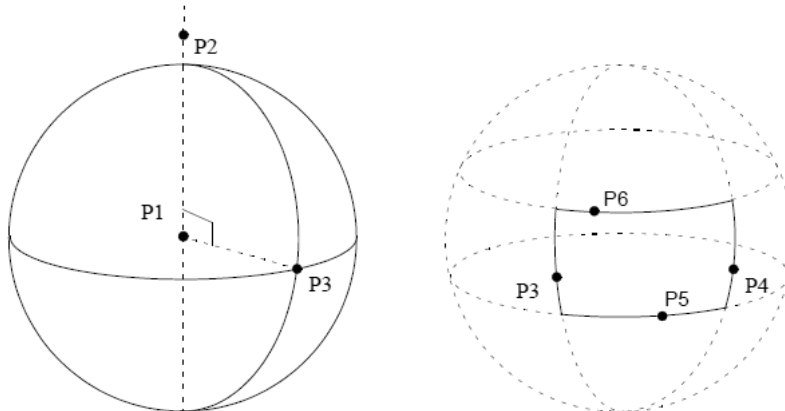

Figure 18. Definition points for a spherical shell in ESATAN-TMS[8].

Following this approach, a number of matrixes equal to the number of needed points must be defined. Each matrix should have *3n* elements, where *n* is the number of shells to be implemented for the approximation and the *3* represents the three Cartesian coordinates x, y, z of the node.

```
REAL P1[52, 3] = {0.0, 0.0, -0.000923179214403, 0.0, 0.0, -0.0027695376432082, ...
REAL P2[52, 3] = {0.0, 0.0, 0.0, 0.0, 0.0, 0.0, ...
REAL P3[52, 3] = {0.0611069739052909, 0.0, -0.000923179214403,
                  0.0611992116768011, 0.0, -0.0027695376432082, ...
REAL P4[52, 3] = {0.0, 0.0610697764855906, 0.001208641571195,
                  0.0, 0.0609790160629047, 0.00241728314239, ...
REAL P5[52, 3] = {0.0, 0.0611, 0.0, 0.0, 0.06106997764855906, 0.001208641571195, ...
```

For each definition point, the position coordinates should be stored in the following order: x-coordinate of the P_X point of the first shell, y-coordinate of the same point, z-coordinate of the same point, x-coordinate of the P_X point of the second shell, and so on. It is important to use the highest possible accuracy in the definition of the coordinates, in order to avoid gaps or overlapping shells.

Once the matrixes of the points have been declared, it is possible to recall them inside a FOR DO loop for the definition of the shells:

```
SHELL Approximation;
SHELL Segments[52];

FOR (n = 1; n <= 52; n = n + 1)
    Segments[n] = SHELL_SPHERE(point1 = [P1[n, 1], P1[n, 2], P1[n, 3]],
                               point2 = [P2[n, 1], P2[n, 2], P2[n, 3]],
                               point3 = [P3[n, 1], P3[n, 2], P3[n, 3]],
                               point5 = [P5[n, 1], P5[n, 2], P5[n, 3]],
                               point6 = [P6[n, 1], P6[n, 2], P6[n, 3]],
                               ...
                               );
END_FOR

Approximation = Segments[1] + Segments[2] + Segments[3] + Segments[4] + ...
```

B. Example
The example herein presented consists of a Stavroudis reflective baffle[9]. This optical device is optimized to reflect all the environmental radiation with an incident angle between 90° and a specified angle from the axis boresight. The device consists of a series of ellipsoids and hyperboloids; the 2D cross section of a baffle which makes use of the Stavroudis concept is reported in Figure 19. The optical functioning of this device is irrelevant to the following discussion, but it is important to know that, assuming perfect shapes and implementing a perfect specular reflectivity (diffusive reflectivity is zero), no environmental radiation coming from the defined range of directions is able to reach the inner side of the front ring and the rear clear aperture of the device (see Figure 20).
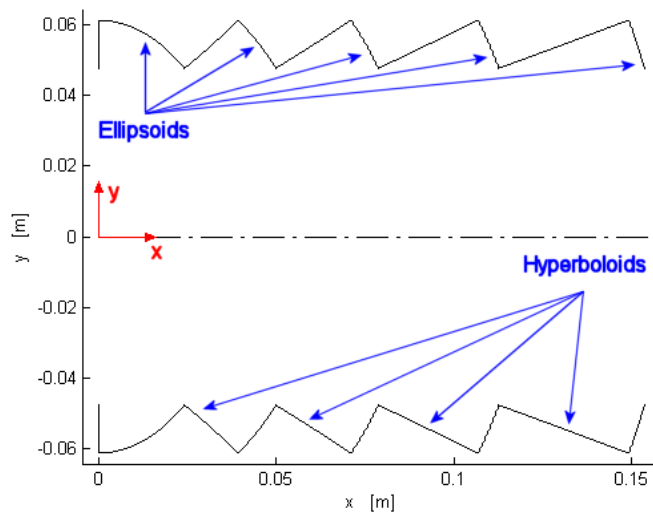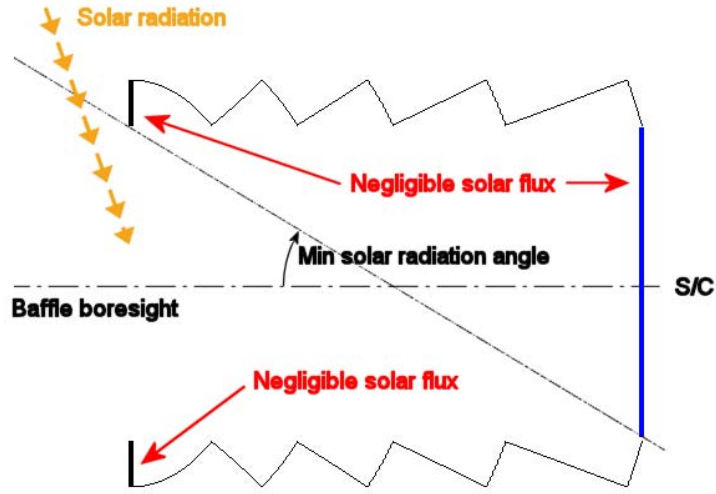

Figure 19. Stavroudis baffle geometry.

Figure 20. Functioning of the Stavroudis baffle.

The first step is the expression of the analytic curves of the cross section in a suitable reference system. As can be seen in Figure 19, the origin of the system has been placed at the beginning of the shape, the x axis aligned with the axis boresight, which is also the axis of the surface of revolution.

The hyperboloids have negative Gaussian curvature[10,11]: this means that the local center of curvature lays *outside* the surface of revolution. Spheres and paraboloids have instead positive Gaussian curvature[12,13] (the local center of curvature lays *inside* the surface of revolution). Cones, which have a Gaussian curvature equal to zero[12], are therefore the only possible solution to represent the hyperbolas without causing asymmetries in the 3D curves. The ellipsoids are instead curves with positive Gaussian curvature[10], and can be represented by any of the previously described curves. Part of the optimization of the discretization consists in finding the most suitable shape.

The equation of the first ellipse is

$$y(x) = \sqrt{b^2 \left(1 - \frac{x^2}{a^2}\right)} \qquad 0 \le x \le x_{END} \tag{24}$$

Deciding to approximate the ellipse using straight lines (cones), and using *n* segments to discretize the x domain, the systems expressed by eq. 26 should be solved:

$$\forall i = 1, \dots n \quad y_{CONE}^{(i)}(x) = a_{CONE}^{(i)} \cdot x + b_{CONE}^{(i)} \tag{25}$$

$$\forall i = 1, \dots n \quad \begin{cases} y_{CONE}^{(i-1)}(x = x_{i-1}) = y(x = x_{i-1}) \\ y_{CONE}^{(i)}(x = x_i) = y(x = x_i) \end{cases} \tag{26}$$

The system has as solution:

$$\forall i = 1, \dots n \quad \begin{cases} a_{CONE}^{(i)} = \dfrac{y_i - y_{i-1}}{x_i - x_{i-1}} \\[2mm] b_{CONE}^{(i)} = \dfrac{x_i \cdot y_{i-1} - x_{i-1} \cdot y_i}{x_i - x_{i-1}} \\[2mm] 0 = x_0 < x_1 < x_2 < \dots < x_{n-1} < x_n = x_{END} \end{cases} \tag{27}$$

21
American Institute of Aeronautics and Astronautics

The *2n* geometrical parameter a_{CONE} and b_{CONE} can be calculated for a homogeneous discretization of the domain (equispaced x_i). Otherwise, the error (eq. 19) can be minimized finding the best value of the x_i parameters. In the showed example, the optimum has been found numerically. The errors ξ_i, which represent the integral error for the *n* segments of the discretization (see eq. 18), have been calculated numerically, then the solution has been iterated, adjusting the discretization in order to reduce the approximation error.

Eq. 28 proved to be an efficient way to reach a solution which is near to the desired minimum. The updated position $x_i^{'}$ of the generic node i is calculated weighting the local error ξ_i on the global error ξ.

$$\forall i = 1, \ldots n \quad x_i^{'} = x_{i-1} + \left(x_i - x_{i-1}\right)\left(\frac{n}{n-1}\right)\left(1 - \frac{\xi_i}{\sum_{i=1}^{n} \xi_i}\right) \tag{28}$$

Defining the approximating cones in ESATAN-TMS using the nodal definition, the following matrixes of points should be adopted:
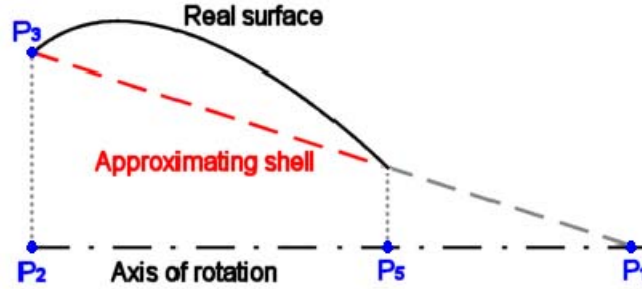

Figure 21. Approximation using cones.

$$\forall i = 1, \ldots n \quad \begin{cases} P_1^{(i)} = \left(-\dfrac{b_{CONE}^{(i)}}{a_{CONE}^{(i)}}, 0, 0\right) \\ P_2^{(i)} = \left(x_{i-1}, 0, 0\right) \\ P_3^{(i)} = \left(x_{i-1}, y_{i-1}, 0\right) \\ P_5^{(i)} = \left(x_i, 0, 0\right) \end{cases} \tag{29}$$

Adopting circumferences instead of straight lines, it's handier to start with the following equations:

$$x^2 + y^2 + \alpha_{CIRC}x + \beta_{CIRC}y + \gamma_{CIRC} = 0 \tag{30}$$

$$y_{CENTER} = -\frac{\beta_{CIRC}}{2} = 0 \quad \rightarrow \quad \beta_{CIRC} = 0 \tag{31}$$

Eq. 31 expresses the condition that the center of the circumference must lie on the axis of rotation.
The systems to be used to identify the geometrical parameters of the approximating curves are:

$$\forall i = 1, \ldots n \quad \begin{cases} y_{CIRC}^{(i-1)}\left(x = x_{i-1}\right) = y\left(x = x_{i-1}\right) \\ y_{CIRC}^{(i)}\left(x = x_i\right) = y\left(x = x_i\right) \end{cases} \tag{32}$$

Which have as solution:

$$\forall i = 1, \ldots n \quad \begin{cases} \alpha_{CIRC}^{(i)} = \dfrac{\left[\left(x^{(i-1)}\right)^2 + \left(y^{(i-1)}\right)^2\right] - \left[\left(x^{(i)}\right)^2 + \left(y^{(i)}\right)^2\right]}{x^{(i)} - x^{(i-1)}} \\[2ex] \beta_{CIRC}^{(i)} = 0 \\[2ex] \gamma_{CIRC}^{(i)} = \dfrac{x^{(i-1)}\left[\left(x^{(i)}\right)^2 + \left(y^{(i)}\right)^2\right] - x^{(i)}\left[\left(x^{(i-1)}\right)^2 + \left(y^{(i-1)}\right)^2\right]}{x^{(i)} - x^{(i-1)}} \\[2ex] 0 = x_0 < x_1 < x_2 < \ldots < x_{n-1} < x_n = x_{END} \end{cases} \tag{33}$$

From eq. 33 it is possible to determinate the position of the center and the radius of the circumferences:

$$\forall i = 1, \ldots n \quad \begin{cases} a_{CIRC}^{(i)} = \dfrac{1}{2}\alpha_{CIRC}^{(i)} \\[2ex] b_{CIRC}^{(i)} = \dfrac{1}{2}\beta_{CIRC}^{(i)} = 0 \\[2ex] r_{CIRC}^{(i)} = \sqrt{\left(\alpha_{CIRC}^{(i)}\right)^2 - \gamma_{CIRC}^{(i)}} \\[2ex] 0 = x_0 < x_1 < x_2 < \ldots < x_{n-1} < x_n = x_{END} \end{cases} \tag{34}$$

The *2n* geometrical parameters a_{CIRC} and b_{CIRC} have been calculated numerically finding the error minimum, in the same way it has been done for the conical approximation.

Defining the spheres in ESATAN-TMS using the nodal definition, the following matrixes of points should be adopted:
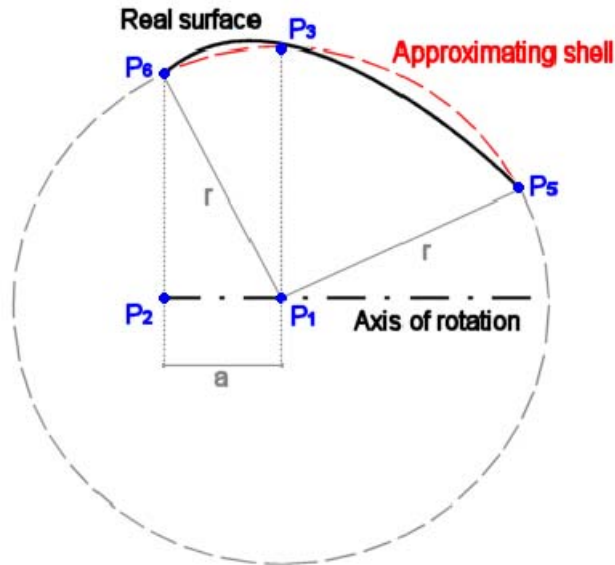

Figure 22. Approximation using circumferences.

$$\forall i = 1, \ldots n \quad \begin{cases} P_1^{(i)} = \left(a_{CIRC}^{(i)}, 0, 0 \right) \\ P_2^{(i)} = (0, 0, 0) \\ P_3^{(i)} = \left(a_{CIRC}^{(i)}, r_{CIRC}^{(i)}, 0 \right) \\ P_5^{(i)} = (x_i, 0, y_i) \\ P_6^{(i)} = (0, 0, y_{i-1}) \end{cases} \tag{35}$$

C. Optimization with respect to environmental fluxes

Performing an optimization using performance indexes based on the geometry, like the condition expressed in eq. 19, it is not possible to easily estimate the performances in terms of optical behavior. The best trade-off between performances and computational cost has to be found a posteriori, comparing the results of simulations applying different discretizations.

Optical devices are often optimized in order to achieve particular radiative behaviors. In many cases, it is possible to analytically calculate the amount of environmental radiation that reaches or is absorbed by some surface. Performing a numerical simulation, it is possible to numerically calculate the same parameter: the difference between the theoretical and the numerical results is the sum of the errors due to the approximation, due to the stochastic method and to the numerical error. Implementing a very accurate definition of the shells, it is possible to reduce the numerical errors; the inaccuracy due to the stochastic method can be reduced increasing the number of rays fired by the ray-tracing method and implementing more severe accuracy parameters.

The results of different approximations of the geometry described in V-B are reported in Figure 23 and Figure 24.
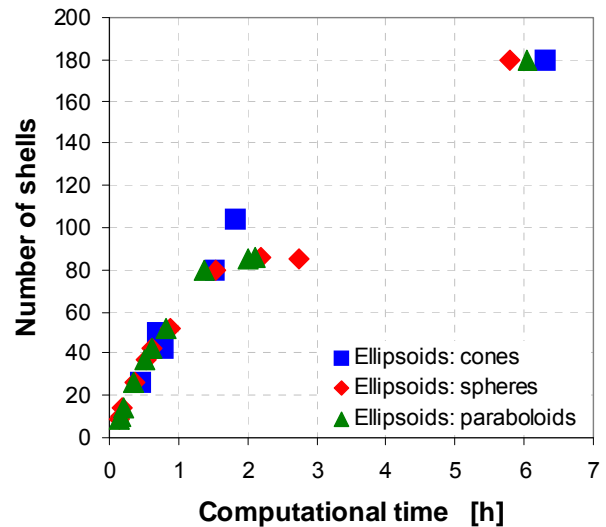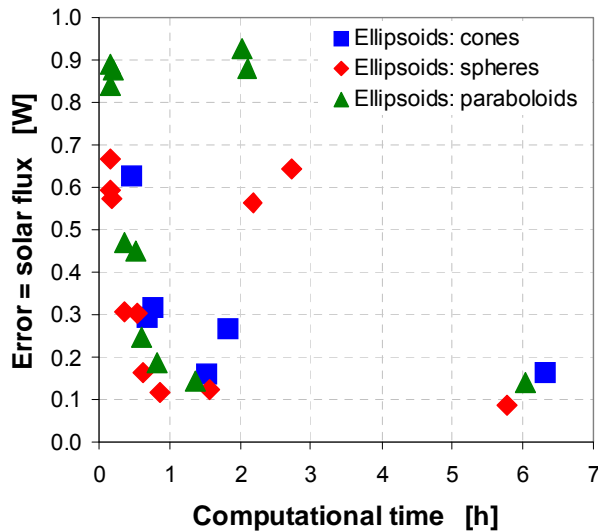

Figure 23. Error parameter vs. computational time.   **Figure 24. Total number of shells vs. computational time.**

The optimal trade-off uses a large number of shells for the approximation of the first ellipsoid, and a quite coarse discretization for the other surfaces. This is due to the fact that the first ellipsoid receives most of the environmental radiation, and therefore a good approximation (in terms of geometrical parameters) of this surface has a stronger influence than a good approximation of the other surfaces.

An important result found is that the best shape to approximate the ellipsoids is the sphere. Using the same number of shells for the approximation, this surface causes the lowest error on the environmental fluxes (see Figure 25). This is in accordance with the results of the geometrical error (defined as in eq. 19), which shows the lowest values when the approximating curve is the circumference (and hence the approximating surface is the sphere).
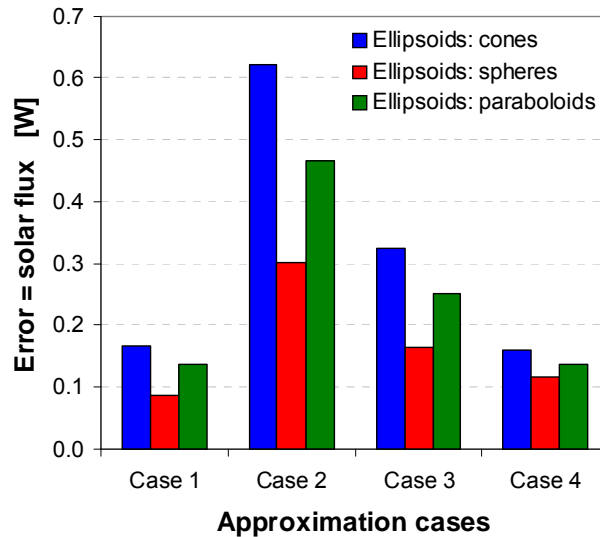
Figure 25. Error parameter vs. approximating surface.

A last observation can be made concerning the minimization of the geometrical error finding the minimum of eq. 19 with respect to the discretization nodes x_i. Simulations which made use of a homogeneous discretization and others with instead an optimized discretization (non homogeneous mesh) showed a little difference, especially if a large number of surfaces were used to discretize the real geometry. The error of the optimized solution was never lower than 98 % with respect to the error of the solution which used a homogeneous discretization.

VI. Conclusion

In this paper, two different topics have been discussed: the implementation of variable thermo-optical properties and the approximation of complex 3D geometries using ESATAN-TMS.

The implementation of temperature-dependant thermo-optical properties for the calculation of the radiative coupling has been illustrated. The procedure is applied in the analysis file directly, in which the radiative exchange factors are dynamically recalculated on the base of the view factor and of a known relation of the emissivity upon the temperature. This method is applicable if no modifications of the specular/diffuse reflectivity ration occur, and if the transmissivity of every surface can be considered constant upon temperature variations. If these conditions are not fulfilled, the radiative model should be modified updating the thermo-optical properties for each time step; the thermal model should then be solved for the given optical properties set and lastly the thermo-optical properties of the radiative model should be updated considering the temperature results from the thermal model. Some iterations are needed to achieve the convergence.

The calculation of the environmental fluxes, taking into account for the wavelength dependency of the optical properties, has also been presented. This method assumes a negligible dependency of the surface absorptivity spectrum upon the temperature of the receiving body. The absorptivity spectrum is weighted upon the environmental radiation to achieve a scalar value to be implemented in the code. A method to estimate the environmental radiation spectrum, based on the equivalent temperature of the source, has also been introduced. If the hypothesis of negligible dependency from the temperature of the absorptivity spectrum is not applicable, then some iterations of radiative solver and thermal solver are needed. For each radiative analysis, the thermal model should be solved using the given set of optical properties, based on the absorptivity spectrum at a given temperature of the body. Once the temperatures have been calculated, it is possible to recalculate the thermo-optical properties weighting the spectra correspondent to the updated temperatures.

An additional example which makes use of an active coating has been presented. The calculation of the environmental fluxes and of the radiative coupling using this type of material has been presented, illustrating a general method to implement variable optical-properties which depend on generic physical quantities or which are user-controlled.

The representation of complex 3D geometries using ESATAN-TMS has been discussed. A general approach to the optimization of the approximation using cones, spheres and paraboloids has been illustrated, as well as the code necessary to implement the approximating shapes. The accuracy of the approximation has been estimated analyzing

the real radiative behavior of the model and comparing the computational results with the results from analytical calculations, in order to achieve a more comprehensible engineering parameter.

The authors cannot provide a mathematical method to properly assess the quality of the approximation on the base of geometry only; on the other hand, the accuracy should be estimated case by case on the basis of the numerical results. The analysis of purely geometrical parameters does not guarantee a good approximation of the radiative behavior of the system. The most important heat fluxes, in terms of absolute value and influence on the system, must be compared with the analytical values, and the results should be compared with the tolerances specific to any single design.

References

[1] Kreith, F., and Bohn, M., *Principles of Heat Transfer*, Thomson Learning, Toronto, Ontario, 2001, Sixth Edition, pp. 571-572

[2] Rohsenow, Warren M., Hartnett, James P., and Cho, Young I. (ed.), *Handbook of Heat Transfer*, McGraw Hill, Boston, Massachusetts, 1998, Third Edition, p. 7.8

[3] Stock, N. J., Kirtley, C. J., De Koning, H. P., and Appel, S., *Automatic Linear Conductor Generation Solution for Lumped Parameter Models*, 35th International Conference On Environmental Systems, July 2005, Rome, Italy

[4] Vilas F., Chapman, C. R., and Matthews, M. S. (ed.), *Mercury*, The University of Arizona Press, Tucson, Arizona, USA, 1988

[5] Hanses, O. L., "Surface temperature and Emissivity of Mercury", *The Astrophysical Journal*, No. 190, 1974 June 15, pp. 715-717

[6] Demiryont, H., and Moorehead, D., "Electrochromic emissivity modulator for spacecraft thermal management", *Solar Energy Materials & Solar Cells*, No. 93, 2009 March 26, pp. 2075–2078

[7] Shannon, Kenneth C. III, "Variable Emittance Electrochromic Thermal Control Space Testing", *Spacecraft Thermal Control Workshop*, El Segundo, California, 2009 March, p. 5

[8] Alstom Aerospace, "ESARAD user manual", UM-ESARAD-024, v. 7.0, 2007 October, p. XVI

[9] Stavroudis, O. N., and Foo, L. D., "System of reflective telescope baffles", *Optical Engineering*, Vol. 33, No. 3, 1994 March, pp. 675-680

[10] Ye, X., "The Gaussian and mean curvature criteria for curvature continuity between surfaces", *Computer Aided Geometric Design*, No. 13, 1996, pp. 549-567

[11] Aksu, T., "A finite element formulation for shells of negative Gaussian curvature", *Computers & Structures*, Vol. 57, No. 6, 1995, pp. 973-979

[12] Magid, E., Soldea, O., and Rivlin, E., "A comparison of Gaussian and mean curvature estimation methods on triangular meshes of range image data", *Computer Vision and Image Understanding*, No. 107, 2007, pp. 139-159

[13] Ghosh, B., and Bandyopadhyay, J. N., "Analysis of paraboloid of revolution type shell structures using isoparametric doubly curved shell elements", *Computers & Structures*, Vol. 36, Issue 5, 1990, pp. 791-800